Fast kq-Space Sampling with Motion-Induced Phase in Diffusion MRI

Fast kq-Space Sampling with Motion-Induced Phase in Diffusion MRI

Marica Pesce, Audrey Repetti, and Yves Wiaux
Institute of Sensors, Signals and Systems, Heriot-Watt University,
Edinburgh EH14 4AS, United Kingdom
mp23, a.repetti, y.wiaux@hw.ac.uk

***Abstract*—High spatio-angular resolution diffusion MRI (dMRI) has been shown to provide accurate identification of complex fiber configurations. However, its application in clinics remains limited due to the long acquisition time that it requires. Recently, we have developed a method relying on a kq-space under-sampling scheme to recover the intra-voxel fiber configurations through accelerated acquisitions. In the current work, we generalize our method to consider a more realistic setting. In particular, the phase contamination induced by magnetic field inhomogeneities and motion during the signal acquisition has been included in the kq-space measurement model. Through experiments on realistic synthetic data, we show that the phase contamination does not penalize the recovery of the fiber configuration, when the phase factor is assumed to be perfectly known.**

***Index Terms*—Diffusion MRI, FOD, kq-space, motion, phase contamination**

I. Introduction

Diffusion Magnetic Resonance Imaging (dMRI) is a powerful tool for studying the tissues micro-structure in-vivo and in a non invasive way. It is extensively used in Neuroscience for the study of the neuronal connectivity [1], [2] and in clinics, for the diagnosis of neurodegenerative diseases such as Schizophrenia and Alzheimer's disease [3], [4]. Multiple methods have been proposed to extract information about the fiber orientation from the diffusion volumes. Among them, we can cite, e.g., the Diffusion Tensor Imaging [5], the Diffusion Spectrum Imaging [6] and the q-ball imaging [7].

The signal acquired in dMRI consists on a set of DW-volumes. Each volume is sensitive to diffusion along a specific direction and at a specific intensity, identified by a 3D point $\mathbf{q}$. The associated 3D space is called q-space, and it is defined by the diffusion gradients. DTI is currently the most widely used approach in clinics, since it requires the acquisition of only 6 diffusion volumes. However, DTI is unable to distinguish the presence of multiple fibers in the same voxel. Recently, high angular resolution diffusion imaging (HARDI) methods have been shown to overcome this limitation. These approaches rely on signals acquired by a large number of diffusion gradients. Although more complex fiber configurations can be resolved by using HARDI approaches, their application in clinics is still limited because of the long acquisition time that they require.

In the last decades, Spherical Deconvolution (SD) [8], [9] has started to gain particular attention for the estimation of complex fiber orientations. This approach models the HARDI signal as a spherical convolution between the Fiber Orientation Distribution (FOD) representing the few active fiber orientations, and a kernel representing the response signal of a single fiber [8]–[11]. SD based approaches enable to recover the FOD, by solving a linear inverse problem [12]. Lately, the Compressed Sensing theory has promoted the use of SD methods for the FOD recovery from a reduced number of diffusion gradients (called q-space under-sampling) [9], [12], [13]. Independently, to short the acquisition process in MRI, methods considering a reduced number of Fourier samples have extensively been used during the last decades. These methods are named k-space under-sampling approaches.

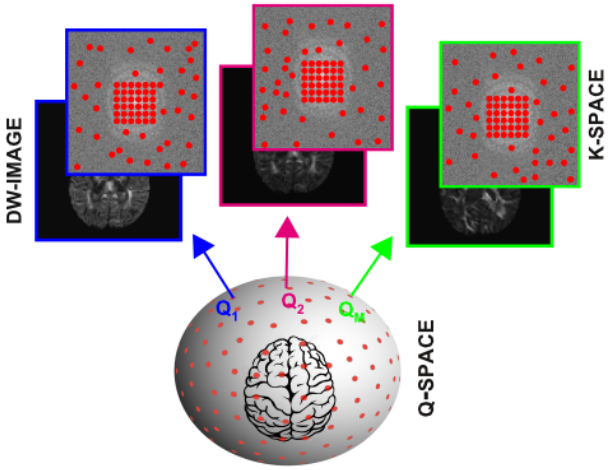

Fig. 1. kq-Space under-sampling approach for dMRI. The dMRI signal is probed by a sequence of diffusion gradients, which identifies a point in the q-space. Each of these points is associated with a specific DW-image and its representation in the k-space. The kq-space method aims at estimating the brain inner structures from the signal generated by a subset of samples in k-space and few samples in q-space.

In this work, we present a method relying on a kq-space under-sampling scheme. This method has been proposed in [14]. As represented in Fig. 1, the dMRI signal is probed by M diffusion gradients, each of which defines a point in the q-space (i.e. q-point). Each q-point is associated with an image, called diffusion weighted (DW) image, and its representation in k-space. The proposed method takes advantage of the under-sampling in both k- and q-space to further reduce the total amount of samples to acquire, thus reducing the acquisition time, while preserving the quality of the estimated FOD.

This work was supported by the UK Engineering and Physical Sciences Research Council (EPSRC, grants EP/M008843/1 and EP/M019306/1).

In general, FOD reconstruction methods acting only in the q-space get rid of the phase, produced by the motion and the magnetic field inhomogeneities, by simply considering the magnitude of the signal. This approach cannot be adopted in the kq-space acquisition context, and FOD reconstruction methods need to explicitly account for the phase contamination in their model. In the present study we show that the phase contamination does not penalize the FOD reconstruction, in the kq-space under-sampling framework.

The remainder of the paper is organized as follows. The proposed method is described in Section II. In Section III we provide the description of the experimental setup and we present the obtained results. Finally, we conclude in Section IV.

II. Proposed kq-space under-sampling approach

A. kq-Space measurement model

In [14], we have proposed to model the FOD reconstruction problem in the kq-space. Let N be the number of imaged voxels. The objective is to find an estimate of the unknown FOD field of interest, $X \in \mathbb{R}^{(n+2)\times N}$, from the observation matrix, $\hat{Y} \in \mathbb{C}^{M\times K}$. Each column of X contains the $n+2$ FOD coefficients of the corresponding voxel. Each row of $\hat{Y}$, denoted by $\hat{Y}_q \in \mathbb{C}^{1\times K}$, corresponds to the under-sampled k-space of the DW-image acquired with gradient $q \in \{1,\ldots,M\}$, and is given by

$$\hat{Y}_q = \mathcal{A}_q(X) + \eta_q, \tag{1}$$

where $\eta_q \in \mathbb{C}^{1\times K}$ is a realization of an i.i.d. Gaussian noise and $\mathcal{A}_q$ is the linear measurement operator, given by

$$\mathcal{A}_q(X) = \Phi_q X S_0 H^{(q)} F M^{(q)}. \tag{2}$$

More precisely, $\Phi_q \in \mathbb{R}^{1\times(n+2)}$ is the q^{th} row of the dictionary $\Phi \in \mathbb{R}^{M\times(n+2)}$ that spans the response of a single fiber oriented along n different directions, to which 2 isotropic compartments, representing the gray matter and the cerebrospinal fluid (CSF), are added. The matrix $S_0 \in \mathbb{R}^{N\times N}$ is a diagonal matrix whose elements correspond to the intensities of the image acquired in the absence of diffusion, named $\mathbf{s}_0$ image. Note that S_0 needs to be taken into account in the model for normalization purposes [14]. The diagonal matrix $H^{(q)} \in \mathbb{C}^{N\times N}$ is used to account for the phase distortions generated by motion and magnetic field inhomogeneities. Finally, $F \in \mathbb{C}^{N\times N}$ represents the 2D Fourier matrix, and $M^{(q)} \in \mathbb{R}^{N\times K^{(q)}}$ is a realization of a random binary mask that under-samples each slice of the acquired volume in a different way.

We refer the reader to [14] for a more general acquisition model, where the multi-coils acquisitions is taken into account.

B. Phase contamination

In MRI, the observed object is inserted in a magnetic field that is made spatially dependent through the application of magnetic field gradients. Additionally, in dMRI the application of the diffusion gradients makes the signal generated by the observed object sensitive to water molecule displacements. Motion of objects placed into magnetic field gradients results in an incorrect phase accumulation. In particular, when the spins of the observed object move along the gradient direction, the acquired signal is characterized by an additional phase. In dMRI, where gradients are large, such motion-induced phase is also large. In the event the observed object undergoes rigid translations, the spins are all subject to the same phase (constant phase accumulation). When the object rotates, the velocities of the spins depend linearly on the position (linear phase accumulation). When the object undergoes non-rigid motion, the motion-induced phase has more complex representation. In general, the motion-induced phase that occurs when imaging the brain results from the combination of rigid and non-rigid motions. Similarly to motion, the presence of magnetic field inhomogeneities contribute to the incorrect accumulation of the phase.

Usually, methods dealing with signals directly in q-space overcome this difficulty by simply taking the magnitude of the complex diffusion signal, in order to obtain real DW-images. However, in k-space, and consequently kq-space, this approach cannot be employed, and the phase factors needs to be modeled in the measurements model. The matrix $H^{(q)}$ in the linear operator expressed in (1) accounts for these factors. Note that, in [14], we have considered synthetic data with linear phase, but without magnetic field inhomogeneities.

In the second column of Fig. 2 we provide the maps of the phase arising from the acquisition of the dMRI signal in the absence of phase contamination (first row), in the presence of phase contamination due only to magnetic field inhomogeneities (second row), and in the presence of phase contamination due to magnetic field inhomogeneities and motion (third row). In the ideal case when the observed object is motionless and inserted in a perfectly homogeneous magnetic field, we can observe that the image recovered from the acquisition system is characterized only by its magnitude (no phase is detected). In this ideal condition, the image is derived from the inverse Fourier transform of a completely symmetric k-space, as it is possible to observe in Fig. 2C and D. In the event the observed object is subject to a magnetic field that is not perfectly homogeneous, we can observe that the obtained DW-image is characterized by complex values with a magnitude (in Fig. 2E) and a phase (in Fig. 2F). In this condition, the symmetry of the k-space is broken by the inhomogeneities as it is shown in Fig. 2G and H. The inverse Fourier transforming of this k-space induces the phase of interest in the image domain. We can observe in Fig. 2L the phase produced when the observed object makes small rotations while it is inserted into an inhomogeneous magnetic field. Finally, by comparing the k-space magnitude and its profile in Fig. 2C,G, and M, it can be observed the effects introduced by motion and magnetic field inhomogeneities in the k-space. The k-space is slightly spread when magnetic field inhomogeneities are considered, while a shift of the k-space occurs when considering rotating objects.

C. Minimization problem and Algorithm

In our approach, we propose to explicitly take advantage of the prior knowledge of tissue distributions over the space

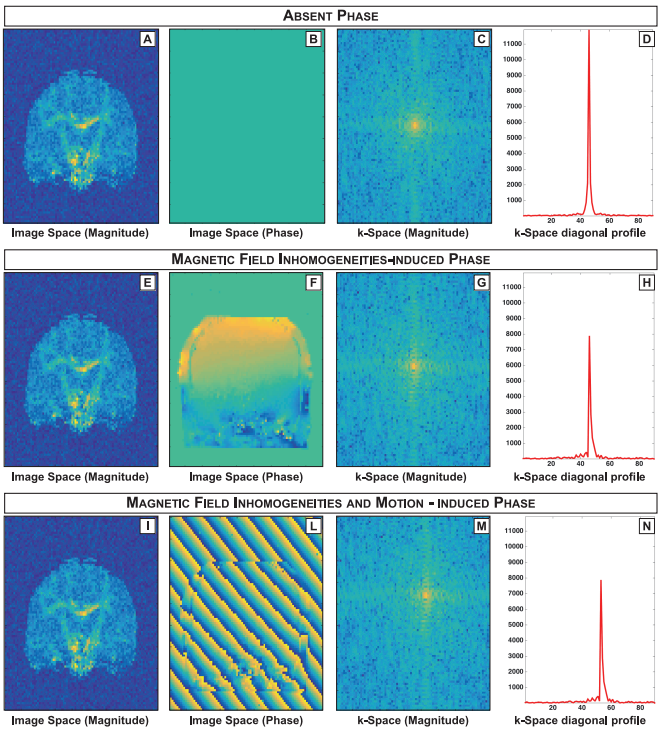

Fig. 2. Visualization of the effects produced in the k-space and in the q-space, by magnetic field inhomogeneities and motion during the diffusion encoding gradients. Magnitude (first column) and phase (second column) of one image of the phantom proposed in the *ISMRM 2015 CHALLENGE* in three different settings. In the first row the observed objects is motionless and inserted into a perfectly homogeneous magnetic field. In the second row magnetic field inhomogeneities are taken into account while the object is assumed to be motionless. In the third row both the inhomogeneities of the magnetic field and the motion of the object are considered. The magnitude of the k-space (logarithmic scale) and the profile of the diagonal line of each k-space is provided in the third and fourth column, respectively.

in order to further regularize the ill-posed FOD estimation problem in (2) [14]. To this aim, we propose to estimate only the subparts of X where the white matter, the gray matter and the CSF are expected. More precisely, let $S_1 \in {\mathbb{R}_+}^{n\times N_1}$ be the variable containing the $N_1 \leq N$ effective FODs associated with the white matter fiber; let $S_2 \in {\mathbb{R}_+}^{1\times N_2}$ be the variable modeling the isotropic behavior characterizing the gray matter tissue, with $N_2 \leq N$ active voxels; and let $S_3 \in {\mathbb{R}_+}^{1\times N_3}$ be the variable modeling the isotropic behavior of the CSF, with $N_3 \leq N$ active voxels.

The object X is fully characterized by $S = (S_1, S_2, S_3)$ through the linear mapping $X = \mathcal{Z}(S)$, where the operator $\mathcal{Z}$ concatenates the matrices resulting from the expansions of S_1, S_2 and S_3 with zero-valued columns in the places of the voxels that are known to not contain the corresponding tissue. Using the proposed notation, we have, for every $q \in \{1,\dots,M\}$, $\mathcal{A}_q(X) = \mathcal{A}_q\big(\mathcal{Z}(S)\big)$. In this context, we propose to define the estimate of $X = \mathcal{Z}(S)$ as a solution to

$$\min_{S=(S_1,S_2,S_3)} \left\| \mathcal{A}\big(\mathcal{Z}(S)\big) - \hat{Y} \right\|_2^2 \text{ s.t. } \begin{cases} S_1 \in \mathcal{B}^+_{1,W}(\kappa), \\ S_2 \in \mathbb{R}_+^{1\times N_2}, \\ S_3 \in \mathbb{R}_+^{1\times N_3}, \end{cases} \tag{3}$$

Algorithm 1 FISTA to solve (3)

1: Let $S^{(0)} = (S_1^{(0)}, S_2^{(0)}, S_3^{(0)}) \in {\mathbb{R}_+}^{n\times N_1} \times {\mathbb{R}_+}^{1\times N_2} \times {\mathbb{R}_+}^{1\times N_3}$.
2: Let $W^{(t)} \in \mathbb{R}_+^{n\times N_1}$, $\zeta^{(0)} = 1$, $\kappa > 0$ and $\gamma \in]0, 1/\|\mathcal{A}[$.
3: **Iterations:**
4: **For** $j = 0, 1, \dots$
5: $\quad \widetilde{S}^{(j)} = S^{(j)} - \gamma \mathcal{Z}^\dagger\Big(\mathcal{A}^\dagger\Big(\mathcal{A}\big(\mathcal{Z}(S^{(j)})\big) - \hat{Y}\Big)\Big)$
6: $\quad \check{S}^{(j)} = \mathcal{P}_{\mathcal{B}^+_{1,W^{(t)}}(\kappa)\times\mathbb{R}_+^{1\times N_2}\times\mathbb{R}_+^{1\times N_3}}\left(\widetilde{S}^{(j)}\right)$
7: $\quad \zeta^{(j+1)} = \frac{1+\sqrt{1+4(\zeta^{(j)})^2}}{2}$
8: $\quad S^{(j+1)} = \check{S}^{(j)} + \frac{\zeta^{(j)}-1}{\zeta^{(j+1)}}\big(\check{S}^{(j)} - S^{(j+1)}\big)$
9: **end for**

where $\mathcal{A}\big(\mathcal{Z}(S)\big) = \Big(\mathcal{A}_q\big(\mathcal{Z}(S)\big)\Big)_{1\leq q\leq M} \in \mathbb{C}^{M\times k}$, $W = (W_{d,v})_{d,v} \in \mathbb{R}_+^{n\times N}$, and $\mathcal{B}^+_{1,W}(\kappa)$ denotes the intersection of the real positive orthant $\mathbb{R}_+^{n\times N}$ with the weighted ℓ_1 ball of radius $\kappa \geqslant 0$, centered in 0. The positive weighted ℓ_1 ball is defined as $\mathcal{B}^+_{1,W}(\kappa) = \big\{S_1 \in \mathbb{R}_+^{n\times N} \,\big|\, \|S_1\|_{1,W} \leqslant \kappa\big\}$, $\|\cdot\|_{1,W}$ being the weighted ℓ_1 norm.

In order to mimic the ℓ_0 pseudo-norm [15], problem (3) is solved $T \geq 1$ times using FISTA [16], [17], using different weighted matrices W. The iterations of FISTA are described in Algorithm 1. Basically, this algorithm is alternating between a gradient step (step 5) and a projection step (step 6). The projection of $\widetilde{S}$ into the closed convex non-empty set $\mathcal{C}$ is defined as $\mathcal{P}_{\mathcal{C}}(\widetilde{S}) = \text{argmin}_{S\in\mathcal{C}}\|S - \widetilde{S}\|_2$. For each cycle $t \in \{1,\dots,T\}$, the weighting matrix $W^{(t)}$ is chosen following the method developed in [18]. Weights designed in [18] promotes simultaneously voxelwise sparsity by forcing to zero spurious peaks though large weights. In addition, these weights enforce the spatial smoothness of fiber orientation by averaging the FOD coefficients over neighbor voxels.

Once the solution is found, a post-processing procedure is performed along the columns of S_1 in order to extract the directions of the fibers within each voxel.

III. Experimental Setup and Results

We analyze the fiber configurations recovered using the proposed kq-space under-sampling approach in the presence of magnetic field inhomogeneities and motion during the diffusion encoding gradients in the case of synthetic data. We consider the realistic numerical phantom proposed in the *ISMRM 2015 Challenge* [19] for the signal in q-space. The phantom consists of a volume of $N = 90x90x60$ voxels, acquired by using $M = 30$ diffusion gradients distributed over a single shell with b-value=$1000mm/s^2$. In our experiments we evaluate the FOD reconstruction for three different settings: in the absence of phase contamination, in the presence of phase contamination only due to magnetic field inhomogeneities, and in the presence of phase contamination due to magnetic field inhomogeneities and motion. The field maps made available in the contest provide the phase contamination induced only by the magnetic field inhomogeneities. When considering only this phase, the same phase map is applied to all the DW-images, regardless of head motion. In each

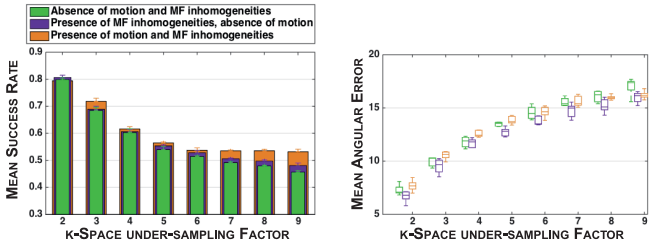

Fig. 3. Quantitative FOD reconstruction evaluation. Bar graph representing the mean success rate (left) and boxplot graph representing the mean angular error (right) at different k-space under-sampling factors (along the x-axis) for three different settings. The FOD reconstruction are performed in the absence of phase contamination (green), in the presence of phase induced by only magnetic field inhomogeneities (purple), and in the presence of phase induced by both magnetic field inhomogeneities and motion (orange).

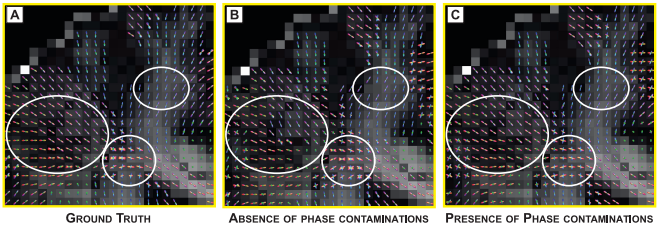

Fig. 4. Qualitative FOD reconstruction evaluation. The FOD reconstructions have been performed on the *ISMRM 2015 CHALLENGE* phantom by considering 30 diffusion gradients, at a k-space under-sampling factor of 9, in the absence (B) and in the presence (C) of motion and magnetic field inhomogeneities. The fiber configuration recovered using 30 gradients, with full k-space, in the absence of phase contamination is provided in A.

voxel $v \in \{1, \dots, N\}$, the intensity of the signal in q-space is multiplied by $e^{i\theta_v}$, θ_v being the value associated with v in the map. When considering motion, a linear phase is added to the phase induced by the magnetic field inhomogeneities. Different linear phase maps are generated for each slice of the phantom and DW-image. The linear phase maps have been modeled in such a way that the corresponding k-space shift does not exceed 20 voxels.

The signal in q-space is then converted to k-space through the Fourier transform and selection masks are applied to the k-space of the DW-images in order to assess the FOD recovery in the kq-space under-sampling setting. The selection masks are built following a variable density sampling approach [20], [21] where the center is fully acquired and the samples in the periphery follow a Gaussian distribution with $\sigma = 0.5$. FODs are recovered solving the problem in (3) where $H^{(q)}$ is known and $\kappa = 4N_1$.

The FOD reconstruction performances are evaluated by taking into account the mean success rate (SR) and the mean angular error indices. The mean SR expresses the portion of voxels in which the number of fibers is correctly estimated. When fibers are individuated, the mean angular error quantifies the angular accuracy with which the fibers orientations are recovered. The fiber configuration recovered from all the available diffusion gradients (i.e. 30 diffusion gradients) with complete k-space is considered as ground truth.

Fig. 3 provides the FOD reconstruction performances obtained with the proposed method when considering different k-space under-sampling factors (along the x-axis) in the case of 3 different settings. In green, purple and orange are respectively reported the performances obtained in the absence of phase contamination, in the presence of phase contamination due to magnetic field inhomogeneities only, and in the presence of phase contamination due to both inhomogeneities and motion. We can observe that fiber reconstructions obtained by considering the phase contamination outperform the ones obtained in its absence. The presence of magnetic field inhomogeneities positively affects the FOD recovery only slightly. The SR increases no more than 3% and the mean angular error drops of 2° when taking into account only the magnetic field inhomogeneities. When considering the phase contaminations induced by inhomogeneities of the magnetic field and the motion of the patient, more significant effects can be appreciated, especially at high k-space under-sampling factors. For instance, in the presence of a k-space under-sampling factors of 9, the SR increases of 8%, when considering both motion and magnetic field inhomogeneities. This quality improvement is only observed for high k-space under-sampling factors. These observations can be interpreted as follows. On the one hand, introducing a linear phase in the observation model corresponds to a Fourier space shifting. On the other hand, for high k-space under-sampling factors, the masks $M^{(q)}$ are mainly selecting frequencies at the center. Consequently, the linear phase allows to measure not only the low frequencies for severe k-space under-sampling, but also part of the higher frequencies, which would not be probed in the absence of phase contamination. This can be interpreted in the CS framework as minimizing the coherence of the measurement operator $\mathcal{A}$.

In Fig. 4 we give a qualitative comparison of the fiber configurations recovered by using 30 diffusion gradients at a k-space under-sampling factor of 9. The reconstructions obtained in the absence and in the presence of phase contamination (due to magnetic field inhomogeneities and motion) is reported in Fig. 4B and C, respectively. In Fig. 4, we can observe that the fiber configuration recovered in the presence of the phase contamination (Fig. 4C) appears smoother and more similar to the ground truth configuration.

IV. Conclusion

In the context of the kq-space under-sampling approach for dMRI proposed in [14], we have shown that the presence of the phase contamination arising from motion during the signal acquisition, does not penalize the recovery of the fiber configurations. In addition, we have observed that, for high k-space under-sampling factors, when this phase is completely known, more accurate fiber orientation configurations are achieved. In conclusion, we have shown that physiological motion and manufacturing scanner imperfections do not represent a limitation for the kq-space under-sampling method, but they are factors which the method can benefit from.

References

[1] D. Le Bihan, "Looking into the functional architecture of the brain with diffusion mri," *Nature Reviews Neuroscience*, vol. 4, pp. 469–480, 2003.

[2] O. Sporns, G. Tononi, and R. Kötter, "The human connectome: A structural description of the human brain," *PLoS Computational Biology*, vol. 1, no. 4, pp. 0245–0251, 2005.

[3] Y. Zhang, N. Schuff, A.-T. Du, H. J. Rosen, J. H. Kramer, M. L. Gorno-Tempini, B. L. Miller, and M. W. Weiner, "White matter damage in frontotemporal dementia and Alzheimer's disease measured by diffusion MRI," *Brain*, vol. 132, no. 9, pp. 2579–2592, 2009.

[4] H. J. Park, C. F. Westin, M. Kubicki, S. E. Maier, M. Niznikiewicz, A. Baer, M. Frumin, R. Kikinis, F. A. Jolesz, R. W. McCarley, and M. E. Shenton, "White matter hemisphere asymmetries in healthy subjects and in schizophrenia: A diffusion tensor MRI study," *NeuroImage*, vol. 23, no. 1, pp. 213–223, 2004.

[5] P. J. Basser, J. Mattiello, and D. Le Bihan, "MR Diffusion Tensor Spectroscopy and Imaging," *Biophysical journal*, vol. 66, pp. 259–267, 1994.

[6] V. J. Wedeen, P. Hagmann, W. Y. I. Tseng, T. G. Reese, and R. M. Weisskoff, "Mapping complex tissue architecture with diffusion spectrum magnetic resonance imaging," *Magnetic Resonance in Medicine*, vol. 54, no. 6, pp. 1377–1386, 2005.

[7] D. S. Tuch, "Q-ball imaging," *Magnetic Resonance in Medicine*, vol. 52, pp. 1358–1372, 2004.

[8] J. D. Tournier, F. Calamante, D. G. Gadian, and A. Connelly, "Direct estimation of the fiber orientation density function from diffusion-weighted MRI data using spherical deconvolution," *NeuroImage*, vol. 23, no. 3, pp. 1176–1185, 2004.

[9] J. D. Tournier, F. Calamante, and A. Connelly, "Robust determination of the fibre orientation distribution in diffusion MRI: Non-negativity constrained super-resolved spherical deconvolution," *NeuroImage*, vol. 35, no. 4, pp. 1459–1472, 2007.

[10] D. C. Alexander, "Maximum entropy spherical deconvolution for diffusion MRI." *Information processing in medical imaging*, vol. 19, pp. 76–87, 2005.

[11] F. Dell'Acqua, G. Rizzo, P. Scifo, R. A. Clarke, G. Scotti, and F. Fazio, "A Model-Based Deconvolution Approach to Solve Fiber Crossing in Diffusion-Weighted MR Imaging," *IEEE Transactions on Biomedical Engineering*, vol. 54, no. 3, pp. 462–472, 2007.

[12] B. Jian and B. C. Vemuri, "A unified computational framework for deconvolution to reconstruct multiple fibers from diffusion weighted MRI," *IEEE Transactions on Medical Imaging*, vol. 26, no. 11, pp. 1464–1471, 2007.

[13] A. Ramirez-Manzanares, M. Rivera, B. C. Vemuri, P. Carney, and T. Mareei, "Diffusion basis functions decomposition for estimating white matter intravoxel fiber geometry," *IEEE Transactions on Medical Imaging*, vol. 26, no. 8, pp. 1091–1102, 2007.

[14] M. Pesce, A. Repetti, A. Auría, A. Daducci, J.-P. Thiran, and Y. Wiaux, "Fast Fiber Orientation Estimation in Diffusion MRI from kq-Space Sampling and Anatomical Priors," arXiv e-print 1802.02912, 2018. [Online]. Available: http://arxiv.org/abs/1802.02912

[15] E. J. Candes, M. B. Wakin, and S. P. Boyd, "Enhancing sparsity by reweighted L1 minimisation," *Journal of Fourier Analysis and Applications*, vol. 14, no. 5, pp. 877–905, 2008.

[16] P. L. Combettes and V. R. Wajs, "Signal Recovery by Proximal Forward-Backward Splitting," *Multiscale Modeling & Simulation*, vol. 4, no. 4, pp. 1168–1200, 2005.

[17] A. Beck and M. Teboulle, "A Fast Iterative Shrinkage-Thresholding Algorithm for Linear Inverse Problems," *SIAM Journal on Imaging Sciences*, vol. 2, no. 1, pp. 183–202, 2009.

[18] A. Auría, A. Daducci, J.-P. Thiran, and Y. Wiaux, "Structured sparsity for spatially coherent fibre orientation estimation in diffusion MRI," *NeuroImage*, vol. 115, pp. 245–255, 2015.

[19] K. H. M. Hein, P. Neher, J. Christophe, and M. Alexandre, "Tractography based connectomes are dominated by false positive connections," *bioRxiv*, pp. 1–23, 2016.

[20] G. Puy, P. Vandergheynst, and Y. Wiaux, "On variable density compressive sampling," *IEEE Signal Processing Letters*, vol. 18, no. 10, pp. 595–598, 2011.

[21] Z. Wang, S. Member, and G. R. Arce, "Variable density compressed image sampling," *IEEE Transactions on Image Processing*, vol. 19, no. 1, pp. 264–270, 2010.